Journal of Materials Chemistry C

PAPER

View Article Online
View Journal | View Issue

Cite this: J. Mater. Chem. C, 2015, 3, 861

Starburst 4,4′,4″-tris(carbazol-9-yl)-triphenylamine-based deep-blue fluorescent emitters with tunable oligophenyl length for solution-processed undoped organic light-emitting diodes†

Mingquan Yu,[ab] Shumeng Wang,[ab] Shiyang Shao,*[a] Junqiao Ding,*[a] Lixiang Wang,*[a] Xiabin Jing[a] and Fosong Wang[a]

Received 26th September 2014
Accepted 17th November 2014

DOI: 10.1039/c4tc02173h

www.rsc.org/MaterialsC

On the basis of a well-known hole transporting material, namely 4,4′,4″-tris(carbazol-9-yl)-triphenylamine (TCTA), a series of star-shaped deep-blue fluorescent emitters (2P-TCTA, 3P-TCTA, 4P-TCTA and 5P-TCTA) have been successfully developed *via* a simple extension of the oligophenyl chain between two N atoms. When the number of phenyl rings increases, it is found that both the absorption and emission for these TCTA-based starbursts are red-shifted and finally become saturated for 5P-TCTA consisting of a pentaphenyl bridge. Interestingly, on going from 2P-TCTA to 5P-TCTA, the film photoluminescence quantum yield is gradually enhanced from 11.4% to 35.5%. The same trend is also observed for their corresponding solution-processed undoped OLEDs. As a consequence, 5P-TCTA shows the best device performance, revealing a maximum luminescence of 7300 cd m^{-2}, and a peak luminous efficiency of 2.48 cd A^{-1} (2.15 lm W^{-1}; 2.30%) together with CIE coordinates of (0.15, 0.09).

Introduction

Since 1987, organic light-emitting diodes (OLEDs) have attracted tremendous attention due to their potential applications in flat-panel displays and solid-state lightings.[1–10] To achieve full-color displays, three primary RGB luminescent materials with excellent stability, efficiency and color purity are required. With respect to green and red counterparts, it seems to be a big challenge to develop blue emitters, especially deep-blue ones that have a Commission Internationale de l'Eclairage (CIE) y coordinate value of <0.10, because the intrinsic wide bandgap would inevitably result in inefficient charge injection to an emitting layer (EML).[11] Therefore, great efforts should be paid to the design of deep-blue emitters to push forward the commercialization of full-color OLEDs.

In general, OLEDs can be fabricated through either vacuum evaporation or solution processes, such as inkjet printing and spin-coating. Compared with the former, the wet method is superior for realizing low-cost and large-area displays.[12] We note that most reported solution-processed deep-blue OLEDs are based on polymers rather than small molecules.[13–18] The multidispersity of polymers as well as some defects, including monomer sequence, end groups and catalyst residues, may limit their device performance and reproducibility.[19,20] As an alternative, starburst conjugated oligomers, in which several conjugated arms are joined together to a central core, are believed to be capable of preventing these drawbacks given their well-defined structures.[21–32] In addition, when deposited *via* a solution process, they possess relatively good film-forming properties owing to the characteristic star-shaped orientation.

Recently, many starburst deep-blue emitters with different cores, such as benzene,[22] truxene,[23] porphyrin,[24] triazatruxene,[25,26] pyrene,[27] spirofluorene,[28] and triphenylamine (TPA), have been demonstrated. Among them, TPA-core molecules represent a group of very promising deep-blue light-emitting materials since they have suitable highest occupied molecular orbital (HOMO) levels to facilitate the hole injection from the anode to the EML. For example, 4,4′,4″-tris(carbazol-9-yl)-triphenylamine (TCTA), bearing a TPA core and three carbazole end-cappers, has been widely used as the hole-transporting material in OLEDs because of its high hole mobility.[33] By connecting six oligofluorene arms at the periphery of TCTA, monodisperse starburst oligomers were reported to display bright, deep-blue fluorescence both in solution and in the solid state.[30] Their corresponding undoped OLEDs revealed a luminescence up to 1025 cd m^{-2} and a maximum luminous efficiency of 0.47 cd A^{-1} with CIE coordinates of (0.16, 0.07).

[a]State Key Laboratory of Polymer Physics and Chemistry, Changchun Institute of Applied Chemistry, Chinese Academy of Sciences, Changchun, 130022, P. R. China. E-mail: ssyang@ciac.ac.cn; junqiaod@ciac.ac.cn; lixiang@ciac.ac.cn

[b]University of Chinese Academy of Sciences, Beijing, 100049, P. R. China

† Electronic supplementary information (ESI) available. See DOI: 10.1039/c4tc02173h

However, these oligofluorene functionalized oligomers may suffer from the unwanted long wavelength emission under long-term device operation, similar to polyfluorene-based macromolecules.[34–36]

In this paper, we propose a novel strategy for the development of starburst TCTA-based deep-blue fluorescent emitters without oligofluorene. Stemming from TCTA, as indicated in Scheme 1, 2P-TCTA, 3P-TCTA, 4P-TCTA and 5P-TCTA have been successfully designed and synthesized by increasing the number of phenyl rings between two N atoms. Such a simple modification is expected to have several advantages: firstly, the ease of hole injection may be kept in the presence of a TPA core; secondly, the fluorene moiety is no longer adopted in this case, thereby avoiding the risk of spectral instability induced by fluorene; most importantly, the extension of the oligophenyl chain could not only enlarge the conjugation length and thus red-shift the emission from 419 nm of 2P-TCTA to 448 nm of 5P-TCTA, but also significantly improve the film photoluminescence quantum yield (PLQY) from 11.4% to 35.5%. As a result, 5P-TCTA reveals a maximum luminescence of 7300 cd m^{-2}, a maximum luminous efficiency of 2.48 cd A^{-1}, and CIE coordinates of (0.15, 0.09). To the best of our knowledge, the obtained undoped device performance is among the highest for solution processable nonfluorene deep-blue emitters.[37–39]

Results and discussion

Synthesis and characterization

Scheme 1 outlines the synthetic route for TCTA-based deep-blue emitters. Starting from 1,4-dibromobenzene and 4,4′-dibromo-1,1′-biphenyl, the selective C–N coupling reactions were carried out to produce CzPBr and Cz2PBr, which were converted into the corresponding boronic esters CzPBO and Cz2PBO, respectively. They subsequently reacted with 4,4′-dibromo-1,1′-biphenyl to afford the monocoupling products Cz3PBr and Cz4PBr in good yields (72–89%) under room temperature conditions by using $Pd(PPh_3)_4$ as the catalyst, Cs_2CO_3 as the base and toluene–methanol as the solvent.[40] Similar to CzPBO and Cz2PBO, Cz3PBO and Cz4PBO were prepared through Pd-catalyzed Miyaura reactions of Cz3PBr and Cz4PBr. In the case of the synthesis of Cz4PBO, a mixed solvent of *N*,*N*-dimethylformamide (DMF) and mesitylene was used to improve the system solubility, and hence considerably increase the yield from 10% to 91%.

With CzPBO–Cz4PBO in hand, the Suzuki cross-couplings of tris(4-bromophenyl)amine were finally performed to give the desired starbursts 2P-TCTA, 3P-TCTA, 4P-TCTA and 5P-TCTA in moderate yields of 45–55%. The structures of 2P-TCTA–5P-TCTA were fully characterized by ^1H and ^{13}C NMR spectroscopy, MALDI-TOF mass spectroscopy and elemental analysis. Moreover, they were all readily soluble in chloroform,

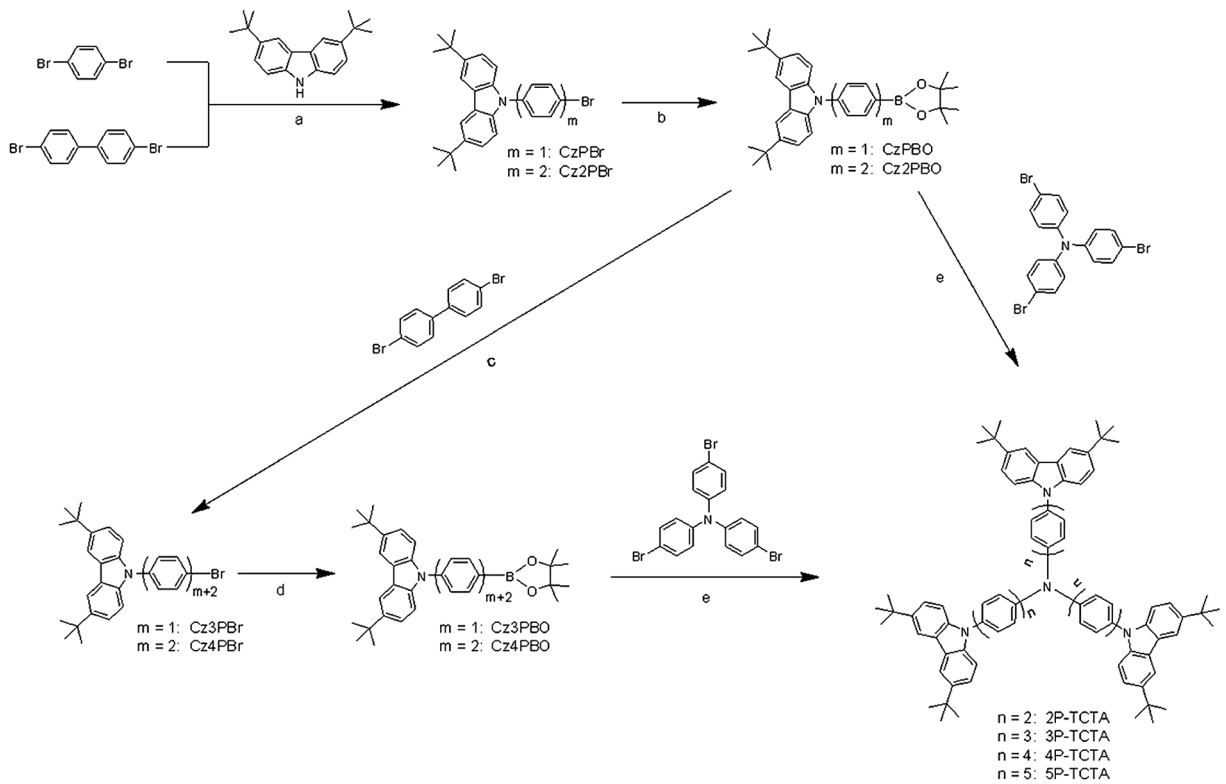

Scheme 1 Synthesis of TCTA-based deep-blue emitters. Reagents and conditions: (a) Cu, CuI, K_2CO_3, *N*,*N*-dimethylethyleneurea (DMI), 140–160 °C; (b) $Pd(dppf)Cl_2$, bis(pinacolato)diboron, KOAc, DMF, 100 °C; (c) $Pd(PPh_3)_4$, Cs_2CO_3, toluene/methanol, room temperature; (d) bis(pinacolato)diboron, $Pd(dppf)Cl_2$, KOAc, DMF/mesitylene, 100 °C; (e) $Pd(OAc)_2$, 2-dicyclohexylphosphino-2′,6′-dimethoxybiphenyl (SPhos), K_2CO_3, Aliquat 336, toluene, reflux.

tetrahydrofuran, chlorobenzene, *o*-dichlorobenzene, and mesitylene, ensuring their capabilities to form high-quality films *via* spin-coating.

Thermal properties

The thermal properties of TCTA-based deep-blue emitters 2P-TCTA–5P-TCTA were measured by thermogravimetric analysis (TGA) and differential scanning calorimetry (DSC). They all exhibit similar decomposition temperatures (T_ds) of 520 °C, corresponding to a 5% weight loss (Fig. 1). When the number of phenyl rings grows, however, the glass transition temperature (T_g) is found to be slightly enhanced from 249 °C for 2P-TCTA to 265 °C for 4P-TCTA. As for 5P-TCTA, no glass transition is observed, and a melting process appears at about 389 °C, which may be tentatively ascribed to the tendency of easy intermolecular packing and hence ready crystallization induced by the extension of the oligophenyl chain. Meanwhile, we note that the T_gs of these TCTA-based derivatives are much higher than those of the deep-blue emitters with oligofluorene arms (60–130 °C),[30,31] indicative of their excellent thermal and morphological stability.

Taking 5P-TCTA as an example, its morphological stability was then investigated by atomic force microscopy (AFM). Fig. 2 compares the AFM images of 5P-TCTA films before and after annealing under vacuum at 150 °C for 2 hours. As one can see, both the pristine and annealed films show a fairly smooth surface morphology with a root-mean-square roughness of 0.408 and 0.722 nm, respectively. The observed good morphological stability is believed to be favorable for the preparation of homogeneous and stable thin films *via* a solution process, thereby improving the reliability of the light-emitting diodes.

Electrochemical properties

Cyclic voltammetry (CV) was used to study the electrochemical properties of 2P-TCTA–5P-TCTA. Upon anodic sweeping in dichloromethane (DCM), all the starbursts show two reversible oxidation waves at 0.4/0.7 V, respectively (Fig. 3). Consistent with the literature,[41] the first oxidation is from the TPA core, while the second corresponds to the carbazole terminals. With regard to the energy level of the ferrocene reference (4.8 eV below the vacuum level), the HOMO levels of 2P-TCTA–5P-TCTA are determined to be about −5.2 eV. The value matches well with that of poly(3,4-ethylenedioxythiopene):poly(styrenesulfonate) (PEDOT:PSS) (−5.1 eV), indicating that the hole-injection from PEDOT:PSS to these emitters would be very efficient. During a cathodic scan in DCM, no reduction waves were detected, and so their lowest unoccupied molecular orbital (LUMO) levels are estimated from the HOMO and optical bandgap (E_g). As tabulated in Table 1, the LUMO decreases gradually from −2.16 eV of 2P-TCTA to −2.29 eV of 5P-TCTA. This is reasonable when considering that the electron could be more delocalized along the extended oligophenyl chain. Furthermore, the low-lying LUMO level for 5P-TCTA means a reduced electron injection barrier, which will be discussed later.

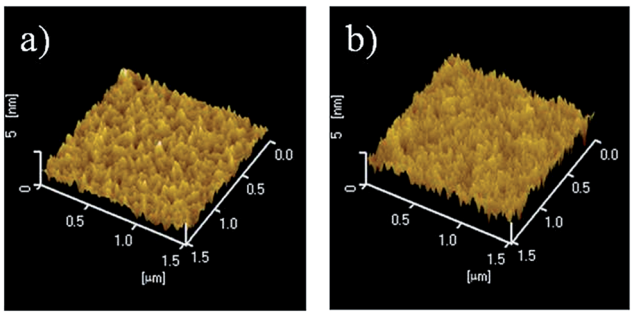

Fig. 2 Comparison of AFM topographic images for 5P-TCTA between the pristine film (a) and annealed film (b).

Photophysical properties

The UV-Vis spectra of 2P-TCTA–5P-TCTA in toluene are shown in Fig. 4a. The low-energy absorption bands in the range of 320–450 nm can be safely attributed to the π–π* transitions of the TPA-core oligophenyl, while the high-energy absorption bands located at 280–320 nm are related to the π–π* transitions of peripheral carbazole moieties.[42] Meanwhile, the absorption onset shows a significant red-shift of 15 nm from 2P-TCTA to 4P-TCTA, but a slight red-shift of 1 nm from 4P-TCTA to

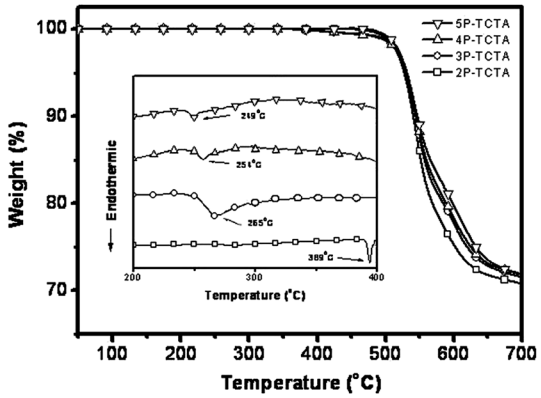

Fig. 1 TGA curves of deep-blue emitters 2P-TCTA–5P-TCTA and their DSC traces (inset).

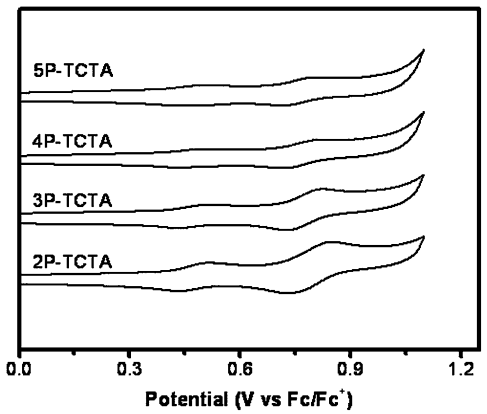

Fig. 3 CV characteristics of deep-blue emitters 2P-TCTA–5P-TCTA.

Table 1 Thermal, electrochemical and photophysical properties of TCTA-based deep-blue emitters

Compound	T_d [°C]	T_g/T_m [°C]	λ_{abs}[a] [nm]	λ^{abs}_{onset}[b] [nm]	E_g[c] [eV]	λ^{s}_{em}[a] [nm]	λ^{f}_{em}[d] [nm]	Φ_{PL}[e] [%]	HOMO[f] [eV]	LUMO[g] [eV]
2P-TCTA	519	249/n.d.	355, 299	396	3.06	404	419	11.4	−5.22	−2.16
3P-TCTA	523	254/n.d.	362, 299	407	2.97	418	434	11.6	−5.21	−2.24
4P-TCTA	520	265/n.d.	355, 299	411	2.94	424	446	22.4	−5.21	−2.27
5P-TCTA	517	n.d./389	353, 299	412	2.93	425	448	35.5	−5.22	−2.29

[a] Measured in toluene with a concentration of 10^{-6} M. [b] Absorption onset taken from the UV-Vis spectra in toluene. [c] Optical bandgap estimated from the absorption onset. [d] Measured in films. [e] Measured in films using an integrating sphere. [f] HOMO = −e(4.8 V + E_{ox}), where E_{ox} is the onset of the first oxidation wave. [g] LUMO = HOMO + E_g.

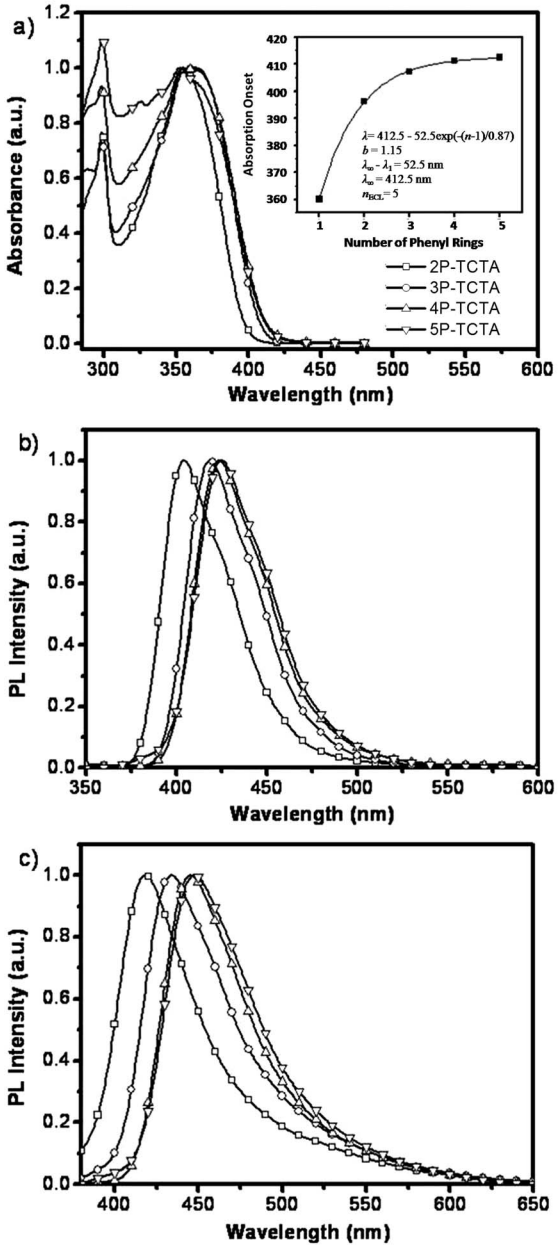

Fig. 4 UV-Vis spectra in toluene (a), PL spectra in toluene (b), and PL spectra in solid states (c) for deep-blue emitters 2P-TCTA–5P-TCTA. Inset: Correlation of the absorption onset and number of phenyl rings.

5P-TCTA (Table 1), implying the conjugation saturation for 5P-TCTA with five benzene units between two N atoms. To further verify this trend, the effective conjugation length (ECL) is then estimated. According to the theory proposed by Meier *et al.*,[43] the dependence of the absorption onset λ on the number of benzene units n can be described by the exponential function, eqn (1):

$$\lambda(n) = \lambda_\infty - (\lambda_\infty - \lambda_1)e^{-b(n-1)} \quad (1)$$

λ_1 belongs to the parent compound TCTA ($\lambda_1 = 360$ nm);[42] λ_∞ is the limiting value for $n = \infty$. And the maximum conjugation is virtually reached for an n_{ECL}, which fulfills eqn (2):

$$\lambda_\infty - \lambda_{ECL} \leq 1 \text{ nm} \quad (2)$$

By applying the above eqn (1) and (2), we find $\lambda_\infty = 412.5$ nm and $n_{ECL} = 5$ (inset of Fig. 4a). The result correlates well with both the absorption and photoluminescence (PL). As indicated in Fig. 4b and c, the emission maxima in both solutions and films display a bathochromic shift with the extended oligophenyl chain, and become saturated for 5P-TCTA at 425 and 448 nm, respectively. These observations suggest that a pentaphenyl bridge is enough to tune the conjugation of TCTA-based starbursts.

On going from solution to film, in addition, the PL spectra of 2P-TCTA–5P-TCTA are all found to be red-shifted by about 15–23 nm, indicative of the existence of aggregation to some degree. Noticeably, 2P-TCTA–5P-TCTA possess significant spectral stability since no fluorene unit is used here for the composition of the blue emitters. For example, even after annealing at 150 °C for 2 hours in air, the PL spectrum of the 5P-TCTA film remains nearly unchanged without the appearance of a low-energy green emission band observed in polyfluorene-based macromolecules (Fig. 5).[34–36] Furthermore, the corresponding film PLQY is measured to be 11.4%, 11.6%, 22.4% and 35.5% for 2P-TCTA, 3P-TCTA, 4P-TCTA and 5P-TCTA, respectively. Compared with 2P-TCTA, the PLQY of 5P-TCTA is improved by about three fold when the number of phenyl rings increases. The reason is not very clear now, but the same phenomenon has been previously reported for 4P-NPD with a tetraphenyl bridge, which has a much higher film PLQY than that of α-NPD with a biphenyl bridge.[44]

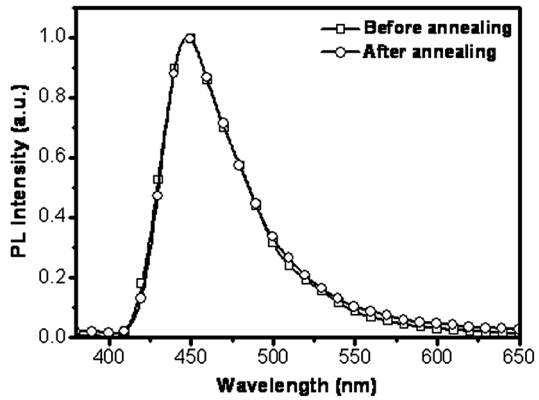

Fig. 5 PL spectra of a 5P-TCTA film before and after annealing at 150 °C for 2 hours in air.

Electroluminescence properties

To investigate the electroluminescence (EL) properties of 2P-TCTA–5P-TCTA, solution-processed undoped OLEDs were fabricated with the configuration of ITO/PEDOT:PSS/2P-TCTA–5P-TCTA/TPBI/LiF/Al. Here, TPBI stands for 1,3,5-tris(1-phenyl-benzimidazol-2-yl)benzene, which acts as the electron transporting layer. Fig. 6 portrays their EL spectra at a driving voltage of 6 V. Noticeably, the EL spectra of 3P-TCTA–5P-TCTA are similar to their PL counterparts in solid states, whereas 2P-TCTA exhibits a much broader EL spectrum relative to its PL one. The possible formation of an exciplex at the interface between the EML and TPBI may contribute to the wideness of the EL spectrum for 2P-TCTA.[31] Despite this difference, all of them display a bright deep-blue emission with CIE coordinates of (0.16, 0.05) for 2P-TCTA, (0.16, 0.08) for 3P-TCTA, (0.15, 0.09) for 4P-TCTA and (0.15, 0.09) for 5P-TCTA.

The current density–voltage–brightness characteristics and luminous efficiency *versus* current density curves of 2P-TCTA–5P-TCTA are depicted in Fig. 7a and b, respectively. And the related data are also summarized in Table 2. It should be noted that all these deep-blue emitters show turn-on voltages below 5 V. This is consistent with their high-lying HOMO levels close to PEDOT:PSS, favorable to the hole injection. Moreover, the turn-on voltage is obviously down from 4.4 V of 2P-TCTA to 3.3 V of 5P-TCTA. With respect to 2P-TCTA (−2.16 eV), the above-mentioned decreased LUMO level of 5P-TCTA (−2.29 eV) can facilitate electron injection and transporting, thus leading to the reduction of the turn-on voltage.[31] Consequently, the brightness as well as current density at the same driving voltage seem to be enhanced monotonically from 2P-TCTA to 5P-TCTA (Fig. 7a).

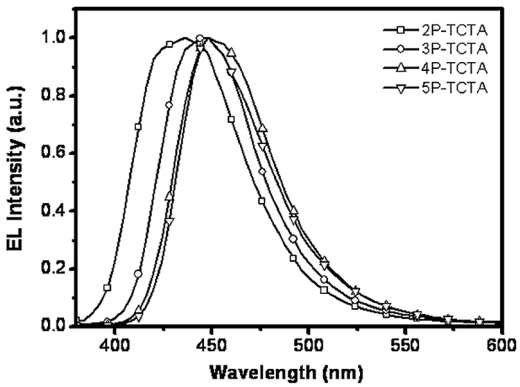

Fig. 6 EL spectra for deep-blue emitters 2P-TCTA–5P-TCTA at a driving voltage of 6 V.

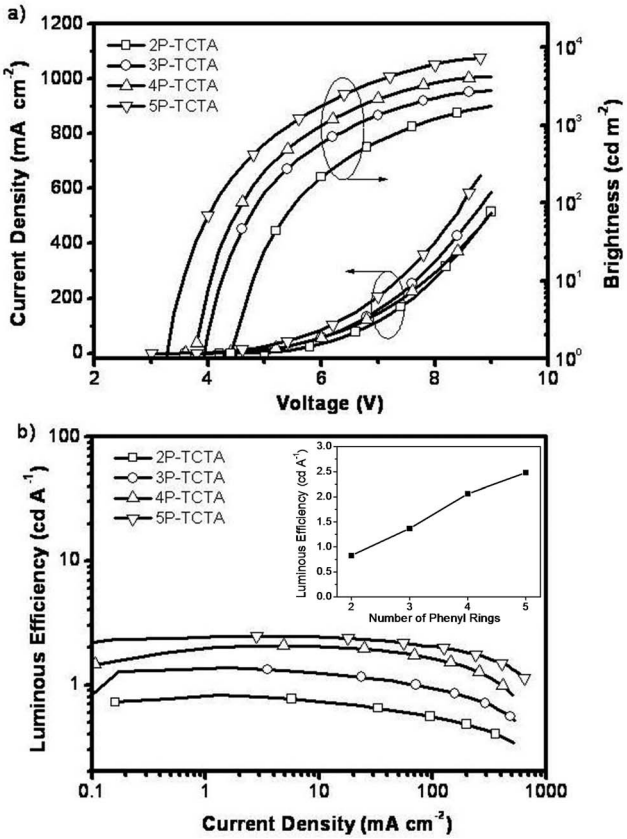

Fig. 7 The current density–voltage–brightness characteristics, and the current density dependence of the luminous efficiency for deep-blue emitters 2P-TCTA–5P-TCTA. Inset: correlation of the luminous efficiency and number of phenyl rings.

Most interestingly, the device performance is found to increase with an increasing number of phenyl rings between two N atoms (Fig. 7b). For instance, 2P-TCTA reveals a maximum luminous efficiency ($\eta_{c,max}$) of 0.83 cd A^{-1}, a maximum power efficiency ($\eta_{p,max}$) of 0.54 lm W^{-1}, a maximum external quantum efficiency ($\eta_{ext,max}$) of 1.33%, and a maximum luminescence (L_{max}) of 1740 cd m^{-2}. As for 5P-TCTA, these values are up to 2.48 cd A^{-1}, 2.15 lm W^{-1}, 2.30% and 7300 cd m^{-2} for $\eta_{c,max}$, $\eta_{p,max}$, $\eta_{ext,max}$ and L_{max}, respectively. The comprehensive performance of 5P-TCTA is superior to that of the star-shaped oligofluorenes with TCTA as the core (0.47 cd A^{-1}, 1025 cd m^{-2}),[30] and among the highest for solution-processable nonfluorene deep-blue emitters.[37]

Compared with 2P-TCTA, the significant improvement of the device performance for 5P-TCTA could be explained as follows: (1) among 2P-TCTA–5P-TCTA, 5P-TCTA possesses the highest

Table 2 Undoped device performance for TCTA-based deep-blue emitters

Device	V_{on}[a] [V]	L_{max}[b] [cd m^{-2}]	$\eta_{c,max}$[c] [cd A^{-1}]	$\eta_{p,max}$[d] [lm W^{-1}]	$\eta_{ext,max}$[e] [%]	CIE[f] [x, y]
2P-TCTA	4.4	1740	0.83	0.54	1.33	(0.16, 0.05)
3P-TCTA	3.9	2795	1.37	1.00	1.57	(0.16, 0.08)
4P-TCTA	3.8	4270	2.06	1.51	2.00	(0.15, 0.09)
5P-TCTA	3.3	7300	2.48	2.15	2.30	(0.15, 0.09)

[a] Turn-on voltage. [b] Maximum luminance. [c] Maximum current efficiency. [d] Maximum power efficiency. [e] Maximum external quantum efficiency. [f] Commission Internationale de l'Eclairage coordinates.

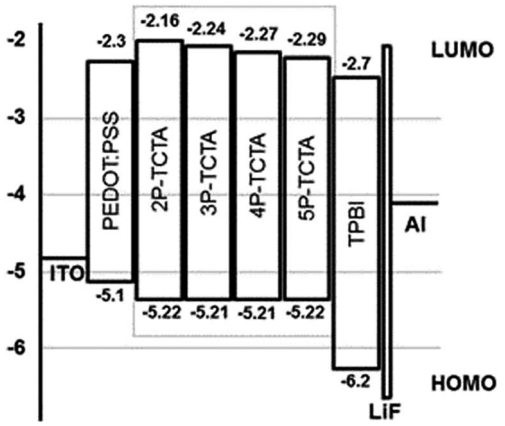

Fig. 8 Energy level diagrams of devices based on 2P-TCTA–5P-TCTA.

PLQY in the film, rendering the generated excitons in OLEDs with a high radiative decay constant. (2) The similar high-lying HOMO levels for all these emitters could ensure an effective hole injection from the adjacent PEDOT:PSS layer to the EML (Fig. 8). On the other hand, the gradual reduction of the LUMO level from 2P-TCTA to 5P-TCTA would lower the electron injection barrier between TPBI and the EML. Therefore, a more balanced charge flux could be anticipated for 5P-TCTA, increasing the recombination possibility of holes and electrons.

Conclusion

In conclusion, by simply tuning the conjugation length of the oligophenyl chain between two N atoms, we have reported a series of star-shaped deep-blue emitters 2P-TCTA–5P-TCTA. They all possess good solution processability and excellent thermal stability. As the number of phenyl rings grows, the film PLQY is up from 11.4% for 2P-TCTA to 35.5% for 5P-TCTA, and the LUMO level is decreased by about 0.13 eV. Solution-processed undoped OLEDs based on these starbursts exhibit bright deep-blue emissions with CIE coordinates ranging from (0.16, 0.05) to (0.15, 0.09). Owing to the highest PLQY as well as the obtained more balanced charge flux induced by the lowered LUMO level, the best device performance is achieved for 5P-TCTA, which gives a state-of-the-art luminous efficiency as high as 2.48 cd A^{-1}. These results suggest that simple extension of the oligophenyl chain could be a promising strategy to optimize the device performance of solution-processed deep-blue OLEDs.

Experimental section

General information

^{1}H NMR and ^{13}C NMR spectra were measured on a Bruker Avance 300 NMR spectrometer or Bruker Avance 400 NMR spectrometer. Elemental analyses of carbon, hydrogen, and nitrogen were performed on a VarioEL elemental analyzer. MALDI-TOF mass spectra were recorded on an AXIMA CFR MS apparatus (COMPACT). Thermal properties of the compounds were analyzed with a Perkin-Elmer-TGA 7 instrument under nitrogen at a heating rate of 10 °C min^{-1}. Differential scanning calorimetry (DSC) was performed on a Perkin-Elmer-DSC 7 instrument at a heating rate of 10 °C min^{-1} from room temperature to 400 °C under nitrogen. The glass transition temperature was determined from the second heating scan. Atomic force microscopy (AFM) images were recorded on a SPA300HV with a SPI3800N controller (Seiko Instruments, Inc., Japan).

Photophysical characterization

The UV/Vis absorption and photoluminescence spectra were measured by a Perkin-Elmer Lambda 35 UV/Vis spectrometer and a Perkin-Elmer LS 50B spectrofluorometer, respectively. Solution spectra were recorded in toluene for UV/Vis absorption with a concentration of 10^{-6} M and for photoluminescence with a concentration of 10^{-5} M. Thin films on quartz for spectroscopic measurements were prepared by drop-coating. The quantum efficiencies of the solid-films were collected by measuring the total light output in all directions in an integrating sphere (C9920-02, HAMAMATSU).

Cyclic voltammetry

All measurements were carried out in dichloromethane with a conventional three-electrode system consisting of a platinum working electrode, a platinum counter electrode, and an Ag/AgCl reference electrode. The supporting electrolyte was 0.1 M tetrabutylammonium perchlorate (n-Bu_4NClO_4). All potentials were calibrated against the ferrocene/ferrocenium couple (Fc/Fc^+). The HOMO levels were calculated according to the equation HOMO = $-e[E_{ox} + 4.8\ V]$, where E_{ox} is the initial oxidation peak value, and the LUMO levels were calculated according to the equation LUMO = HOMO + ΔE_g, where ΔE_g is the optical bandgap estimated from the onset of the absorption spectrum.

Device fabrication and measurement

Patterned glass substrates coated with indium tin oxide (ITO) (20 Ω per square) were cleaned with acetone, detergent, distilled water, and then in an ultrasonic solvent bath. After baking in a heating chamber at 120 °C for 8 h, the ITO-glass substrates were treated with O_2 plasma for 25 min. Subsequently, a 40 nm-thick poly(3,4-ethylenedioxythiophene):poly(styrenesulfonate) (PEDOT:PSS, Batron-P4083, Bayer AG) film was spin-coated on top of the ITO and then baked at 120 °C for 40 min. Then, solutions of the deep-blue emitters in *o*-dichlorobenzene or mesitylene were filtered through a filter (0.45 μm) and spin-coated on PEDOT:PSS as the emissive layer (EML). After annealing at 120 °C for 30 min, the thickness of the EML was about 40 nm. Successively, the substrate was transferred to a vacuum thermal evaporator and a 50 nm-thick film of TPBI was evaporated on top of the EML at a base pressure less than 10^{-6} Torr (1 Torr = 133.32 Pa). Finally, 1 nm LiF and 100 nm Al were deposited subsequently as the cathode through a shadow mask with an array of 14 mm^2 openings. The EL spectra and CIE coordinates were measured using a PR650 spectra colorimeter. The current–voltage and brightness–voltage curves of the devices were measured using a Keithley 2400/2000 source meter and a calibrated silicon photodiode. All the measurements were carried out at room temperature under ambient conditions.

Synthesis

1,4-Dibromobenzene, 4,4′-dibromo-1,1′-biphenyl were bought and recrystallized in *n*-hexane before use. All solvents for chemical synthesis were purified according to the standard procedures. Tris(4-bromophenyl)amine[45] and 3,6-di-*tert*-butyl-9*H*-carbazole[46] were prepared according to literature methods.

Synthesis of 9-(4-bromophenyl)-3,6-di-*tert*-butyl-9*H*-carbazole (CzPBr). 3,6-Di-*tert*-butyl-9*H*-carbazole (6.00 g, 21.50 mmol), Cu powder (2.73 g, 42.95 mmol), CuI (0.41 g, 2.15 mmol), and K_2CO_3 (13.67 g, 64.40 mmol) were added to a solution of 1,4-dibromobenzene (10.13 g, 42.95 mmol) in 30 ml *N*,*N*-dimethylethyleneurea (DMI). The mixture was stirred at 160 °C for 12 h. After cooling to room temperature, the solvent was removed under vacuum at 120 °C. The residue was poured into dichloromethane (DCM) and the organic layer was washed with water and then dried over anhydrous Na_2SO_4. After the solvent was removed, the residue was purified by column chromatography on silica gel with *n*-hexane as eluent to get a white solid in 70% yield. ^{1}H NMR (300 MHz, $CDCl_3$): δ 8.13 (d, J = 1.5 Hz, 2H), 7.70 (d, J = 8.6 Hz, 2H), 7.46 (dd, J = 8.3, 1.9 Hz, 2H), 7.43 (d, J = 6.1 Hz, 2H), 7.31 (d, J = 8.6 Hz, 2H), 1.46 (s, 18H).

Synthesis of 9-(4′-bromo-[1,1′-biphenyl]-4-yl)-3,6-di-*tert*-butyl-9*H*-carbazole (Cz2PBr). 3,6-Di-*tert*-butyl-9*H*-carbazole (6.00 g, 21.5 mmol), Cu powder (2.73 g, 42.95 mmol), CuI (0.41 g, 2.15 mmol), and K_2CO_3 (13.67 g, 64.40 mmol) were added to a solution of 4,4′-dibromo-1,1′-biphenyl (10.10 g, 32.21 mmol) in 30 ml DMI. The reaction was carried out at 140 °C for 12 h. After cooling to room temperature, the solution was washed with water and dried with anhydrous sodium sulfate. The residue was dissolved in dichloromethane and purified by column chromatography on silica gel with *n*-hexane as eluent to get a white solid in 60% yield. ^{1}H NMR (400 MHz, $CDCl_3$): δ = 8.18 (d, J = 1.2, 2H), 7.76 (d, J = 8.4, 2H), 7.64 (dd, J = 8.3, 4.7, 4H), 7.56 (d, J = 8.4, 2H), 7.49 (dd, J = 8.6, 1.7, 2H), 7.42 (d, J = 8.6, 2H), 1.50 (s, 18H).

Synthesis of 3,6-di-*tert*-butyl-9-(4-(4,4,5,5-tetramethyl-1,3,2-dioxaborolan-2-yl)phenyl)-9*H*-carbazole (CzPBO). CzPBr (5.40 g, 12.43 mmol), bis(pinacolato)diboron (7.89 g, 31.08 mmol), Pd(dppf)Cl_2 (0.18 g, 0.25 mmol), and KOAc (3.66 g, 37.30 mmol) were added to a clean dry three-neck flask filled with argon. 30 ml *N*,*N*-dimethylformamide (DMF) was added into the mixture. Then the solution was stirred and heated to reflux at 100 °C for 12 h. After cooling to room temperature, 100 ml water was slowly added to the solution. The mixture was filtered and the residue was washed with water and dried with anhydrous sodium sulfate and then purified by column chromatography on silica gel with *n*-hexane/ethyl acetate (20/1 v/v) as eluent to get a white solid in 96% yield. ^{1}H NMR (300 MHz, $CDCl_3$): δ = 8.13 (d, J = 1.5, 2H), 8.02 (d, J = 8.2, 2H), 7.58 (d, J = 8.2, 2H), 7.46 (dd, J = 8.7, 1.8, 2H), 7.39 (d, J = 8.7, 2H), 1.46 (s, 18H), 1.40 (s, 12H).

Synthesis of 3,6-di-*tert*-butyl-9-(4′-(4,4,5,5-tetramethyl-1,3,2-dioxaborolan-2-yl)-[1,1′-biphenyl]-4-yl)-9*H*-carbazole (Cz2PBO). Cz2PBO was prepared in 95% yield according to a similar procedure to CzPBO by using Cz2PBr instead of CzPBr. ^{1}H NMR (400 MHz, $CDCl_3$): δ = 8.15 (d, J = 1.7, 2H), 7.94 (d, J = 8.1, 2H), 7.82 (d, J = 8.8, 2H), 7.70 (d, J = 8.2, 2H), 7.63 (d, J = 8.4, 2H), 7.47 (dd, J = 8.7, 1.9, 2H), 7.40 (d, J = 8.6, 2H), 1.47 (s, 18H), 1.38 (s, 12H).

Synthesis of 9-(4″-bromo-[1,1′:4′,1″-terphenyl]-4-yl)-3,6-di-*tert*-butyl-9*H*-carbazole (Cz3PBr). CzPBO (5.72 g, 11.92 mmol), 4,4′-dibromo-1,1′-biphenyl (7.44 g, 23.83 mmol), Pd(PPh_3)$_4$ (0.14 g, 0.12 mmol) and Cs_2CO_3 (7.71 g, 23.83 mmol) were added into a round-bottom flask. After 105 ml solvent of methanol–toluene (20 : 1 v/v) was added, the solution was stirred at room temperature and protected under argon for 24 h. 200 ml methanol was added into the flask to precipitate a white solid which was collected by filtration and washed with methanol. The solid was purified by column chromatography on silica gel with cyclohexane/dichloromethane (10/1 v/v) as eluent to get a white solid in 72% yield. ^{1}H NMR (300 MHz, $CDCl_3$): δ = 8.16 (d, J = 1.4, 2H), 7.84 (d, J = 8.4, 2H), 7.78 (d, J = 8.3, 2H), 7.69 (d, J = 8.4, 2H), 7.65 (d, J = 8.4, 2H), 7.61 (d, J = 8.6, 2H), 7.54 (d, J = 8.5, 2H), 7.49 (dd, J = 8.7, 1.7, 2H), 7.43 (d, J = 8.6, 2H), 1.48 (s, 18H).

Synthesis of 9-(4‴-bromo-[1,1′:4′,1″:4″,1‴-quaterphenyl]-4-yl)-3,6-di-*tert*-butyl-9*H*-carbazole (Cz4PBr). Cz4PBr was prepared in 89% yield according to a similar procedure to Cz3PBr by using Cz2PBO instead of CzPBO. ^{1}H NMR (400 MHz, $CDCl_3$): δ = 8.16 (s, 2H), 7.85 (d, J = 7.8, 2H), 7.77 (d, J = 14.2, 6H), 7.67 (t, J = 7.4, 4H), 7.60 (d, J = 8.3, 2H), 7.53 (d, J = 8.3, 2H), 7.49 (d, J = 8.5, 2H), 7.43 (d, J = 8.7, 2H), 1.48 (s, 18H).

Synthesis of 3,6-di-*tert*-butyl-9-(4″-(4,4,5,5-tetramethyl-1,3,2-dioxaborolan-2-yl)-[1,1′:4′,1″-terphenyl]-4-yl)-9*H*-carbazole (Cz3PBO). Cz3PBO was prepared in 95% yield according to a similar procedure to CzPBO by using Cz3PBr instead of CzPBr. ^{1}H NMR (400 MHz, $CDCl_3$): δ = 8.16 (d, J = 1.3, 2H), 7.93 (d, J = 8.0, 2H), 7.84 (d, J = 8.4, 2H), 7.77 (s, 4H), 7.69 (d, J = 8.0, 2H),

7.65 (d, $J = 8.4$, 2H), 7.48 (dd, $J = 8.7$, 1.6, 2H), 7.43 (d, $J = 8.6$, 2H), 1.46 (d, $J = 9.3$, 18H), 1.38 (s, 12H).

Synthesis of 3,6-di-*tert*-butyl-9-(4‴-(4,4,5,5-tetramethyl-1,3,2-dioxaborolan-2-yl)-[1,1′:4′,1″:4″,1‴-quaterphenyl]-4-yl)-9*H*-carbazole (Cz4PBO). Cz4PBr (9.80 g, 14.79 mmol), bis(pinacolato)diboron (7.51 g, 29.58 mmol), Pd(dppf)Cl_2 (0.36 g, 0.44 mmol), and KOAc (4.35 g, 44.3 mmol) were added to a clean dry three-neck flask filled with argon. 50 ml *N*,*N*-dimethylformamide (DMF)–mesitylene (1 : 5) was added into the mixture. Then the solution was stirred and heated to reflux at 100 °C for 24 h. After cooling to room temperature, 100 ml dichloromethane was added to the solution and washed with water. The organic layer was collected and dried with anhydrous sodium sulfate. The solvent was removed under vacuum at 120 °C. The residue was purified by column chromatography on silica gel with *n*-hexane/ethyl acetate (20/1 v/v) as eluent to get a white solid in 91% yield. ^{1}H NMR (400 MHz, $CDCl_3$) $\delta = 8.16$ (d, $J =$ 1.6, 2H), 7.92 (d, $J = 8.2$, 2H), 7.85 (d, $J = 8.4$, 2H), 7.81–7.77 (m, 4H), 7.77–7.72 (m, 4H), 7.68 (d, $J = 8.2$, 2H), 7.65 (d, $J = 8.4$, 2H), 7.49 (dd, $J = 8.7$, 1.9, 2H), 7.43 (d, $J = 8.6$, 2H), 1.48 (s, 18H), 1.38 (s, 12H).

Synthesis of tris(4′-(3,6-di-*tert*-butyl-9*H*-carbazol-9-yl)-[1,1′-biphenyl]-4-yl)amine (2P-TCTA). Tris(4-bromophenyl)amine (1.00 g, 2.07 mmol), CzPBO (3.61 g, 7.47 mmol), $Pd(OAc)_2$ (0.014 g, 0.062 mmol) and SPhos (0.051 g, 0.124 mmol) were dissolved in 50 ml toluene. An aqueous solution of 2 M K_2CO_3 (9.4 ml, 18.67 mmol K_2CO_3) and one drop of Aliquat 336 was added to the solution and then the mixture was heated to 100 °C for 24 h under argon. After reaction, 100 ml DCM was added to the solution after being cooled to room temperature and washed with water and dried with anhydrous sodium sulfate. Solvents were removed under vacuum and the residue was purified by column chromatography on silica gel with *n*-hexane/dichloromethane (5/1 v/v) as eluent to get a white solid in 45% yield. ^{1}H NMR (400 MHz, $CDCl_3$): δ 8.16 (d, $J = 1.7$ Hz, 6H), 7.82 (d, $J = 8.4$ Hz, 6H), 7.67 (d, $J = 8.6$ Hz, 6H), 7.63 (d, $J = 8.5$ Hz, 6H), 7.48 (dd, $J = 8.7$, 1.9 Hz, 6H), 7.42 (d, $J = 8.6$ Hz, 6H), 7.35 (d, $J = 8.5$ Hz, 6H), 1.48 (s, 54H). ^{13}C NMR (101 MHz, $CDCl_3$): $\delta = 147.00$, 142.90, 139.25, 139.09, 137.09, 134.94, 127.97, 127.90, 126.98, 124.63, 123.62, 123.44, 116.26, 109.29, 34.75, 32.03. MS (MALDI-TOF): *m*/*z*: 1304.8. Elemental analysis calcd (%) for $C_{96}H_{96}N_4$: C, 88.30; H, 7.41; N, 4.29; found: C, 87.81; H, 7.24; N, 4.06.

Synthesis of tris(4″-(3,6-di-*tert*-butyl-9*H*-carbazol-9-yl)-[1,1′:4′,1″-terphenyl]-4-yl)amine (3P-TCTA). 3P-TCTA was prepared in 50% yield according to a similar procedure to 2P-TCTA by using Cz2PBO instead of CzPBO. ^{1}H NMR (400 MHz, $CDCl_3$): $\delta = 8.16$ (d, $J = 1.6$, 6H), 7.86 (d, $J = 8.4$, 6H), 7.77 (q, $J =$ 8.5, 12H), 7.65 (d, $J = 8.4$, 12H), 7.49 (dd, $J = 8.7$, 1.8, 6H), 7.43 (d, $J = 8.6$, 6H), 7.32 (d, $J = 7.9$, 6H), 1.48 (s, 54H). ^{13}C NMR (101 MHz, $CDCl_3$): $\delta = 146.93$, 142.92, 139.68, 139.21, 139.14, 138.80, 137.43, 135.04, 128.15, 127.85, 127.45, 127.15, 126.95, 124.56, 123.64, 123.46, 116.25, 109.30, 34.73, 32.03. MS (MALDI-TOF): *m*/*z*: 1532.9. Elemental analysis calcd (%) for $C_{114}H_{108}N_4$: C, 89.25; H, 7.10; N, 3.65; found: C, 89.01; H, 7.7; N, 3.47.

Synthesis of tris(4‴-(3,6-di-*tert*-butyl-9*H*-carbazol-9-yl)-[1,1′:4′,1″:4″,1‴-quaterphenyl]-4-yl)amine (4P-TCTA). 4P-TCTA was prepared in 48% yield according to a similar procedure to 2P-TCTA by using Cz3PBO instead of CzPBO. ^{1}H NMR (400 MHz, $CDCl_3$): $\delta = 8.16$ (d, $J = 1.5$, 6H), 7.86 (d, $J = 8.4$, 6H), 7.80 (s, 12H), 7.76 (dd, $J = 16.1$, 8.5, 12H), 7.64 (t, $J = 8.6$, 12H), 7.49 (dd, $J = 8.7$, 1.8, 6H), 7.43 (d, $J = 8.6$, 6H), 7.31 (d, $J = 8.4$, 6H), 1.48 (s, 54H). ^{13}C NMR (101 MHz, $C_6Cl_2D_4$) $\delta = 147.38$, 143.39, 140.07, 139.83, 139.78, 139.38, 139.32, 138.13, 135.60, 132.73, 128.25, 128.00, 127.50, 127.40, 127.15, 126.90, 124.91, 124.34, 123.87, 116.45, 109.74, 34.71, 32.10. MS (MALDI TOF): *m*/*z*: 1761.0. Elemental analysis calcd (%) for $C_{132}H_{120}N_4$: C, 89.96; H, 6.86; N, 3.18; found: C, 89.70; H, 6.92; N, 2.96.

Synthesis of tris(4⁗-(3,6-di-*tert*-butyl-9*H*-carbazol-9-yl)-[1,1′:4′,1″:4″,1‴:4‴,1⁗-quinquephenyl]-4-yl)amine (5P-TCTA). 5P-TCTA was prepared in 55% yield according to a similar procedure to 2P-TCTA by using Cz4PBO instead of CzPBO. ^{1}H NMR (400 MHz, $C_6Cl_2D_4$): $\delta = 8.45$ (s, 6H), 8.06 (d, $J = 8.2$, 6H), 7.99–7.92 (m, 36H), 7.88 (d, $J = 8.2$, 6H), 7.81 (d, $J = 0.81$, 6H), 7.69 (d, $J = 8.6$, 6H), 7.62 (d, $J = 8.6$, 6H), 7.57 (d, $J = 8.0$, 6H), 1.68 (s, 54H). ^{13}C NMR (101 MHz, $C_6Cl_2D_4$): $\delta = 147.37$, 143.39, 140.03, 139.92, 139.78, 139.64, 139.36, 138.14, 135.42, 132.73, 128.24, 127.99, 127.52, 127.39, 127.14, 126.90, 124.90, 124.34, 123.86, 116.45, 109.73, 34.70, 32.09; MS (MALDI-TOF): *m*/*z*: 1989.0. Elemental analysis calcd (%) for $C_{150}H_{132}N_4$: C, 90.50; H, 6.68; N, 2.81; found: C, 90.44; H, 6.60; N, 2.66.

Acknowledgements

The authors are grateful to the 973 Project (no. 2009CB623601), and the National Natural Science Foundation of China (nos 21174144, 51322308 and 91333205) for financial support of this research.

References

1 C. W. Tang and S. A. VanSlyke, *Appl. Phys. Lett.*, 1987, **51**, 913–915.
2 M. A. Baldo, M. E. Thompson and S. R. Forrest, *Nature*, 2000, **403**, 750–753.
3 B. W. D'Andrade and S. R. Forrest, *Adv. Mater.*, 2004, **16**, 1585–1595.
4 Y. R. Sun, N. C. Giebink, H. Kanno, B. W. Ma, M. E. Thompson and S. R. Forrest, *Nature*, 2006, **440**, 908–912.
5 C. C. Wu, Y. T. Lin, K. T. Wong, R. T. Chen and Y. Y. Chien, *Adv. Mater.*, 2004, **16**, 61–65.
6 S.-J. Su, E. Gonmori, H. Sasabe and J. Kido, *Adv. Mater.*, 2008, **20**, 4189–4194.
7 M. Zhu, Q. Wang, Y. Gu, X. Cao, C. Zhong, D. Ma, J. Qin and C. Yang, *J. Mater. Chem.*, 2011, **21**, 6409–6415.
8 K. T. Kamtekar, A. P. Monkman and M. R. Bryce, *Adv. Mater.*, 2010, **22**, 572–582.
9 Y. Zhang, S.-L. Lai, Q.-X. Tong, M.-F. Lo, T.-W. Ng, M.-Y. Chan, Z.-C. Wen, J. He, K.-S. Jeff, X.-L. Tang, W.-M. Liu, C.-C. Ko, P.-F. Wang and C.-S. Lee, *Chem. Mater.*, 2011, **24**, 61–70.
10 Z. Jiang, Z. Liu, C. Yang, C. Zhong, J. Qin, G. Yu and Y. Liu, *Adv. Funct. Mater.*, 2009, **19**, 3987–3995.

11 M.-T. Lee, H.-H. Chen, C.-H. Liao, C.-H. Tsai and C. H. Chen, *Appl. Phys. Lett.*, 2004, **85**, 3301–3303.
12 A. C. Arias, J. D. MacKenzie, I. McCulloch, J. Rivnay and A. Salleo, *Chem. Rev.*, 2010, **110**, 3–24.
13 G. X. Jiang, C. L. Bian, J. Q. Ding and L. X. Wang, *Chin. J. Polym. Sci.*, 2013, **31**, 787–797.
14 Z. Q. Gao, Z. H. Li, P. F. Xia, M. S. Wong, K. W. Cheah and C. H. Chen, *Adv. Funct. Mater.*, 2007, **17**, 3194–3199.
15 L. H. Xie, X. Y. Deng, L. Chen, S. F. Chen, R. R. Liu, X. Y. Hou, K. Y. Wong, Q. D. Ling and W. Huang, *J. Polym. Sci., Part A: Polym. Chem.*, 2009, **47**, 5221–5229.
16 K. T. Kamtekar, H. L. Vaughan, B. P. Lyons, A. P. Monkman, S. U. Pandya and M. R. Bryce, *Macromolecules*, 2010, **43**, 4481–4488.
17 J. P. Lu, Y. Tao, M. D'Iorio, Y. N. Li, J. F. Ding and M. Day, *Macromolecules*, 2004, **37**, 2442–2449.
18 S. A. Chen and C. I. Chao, *Synth. Met.*, 1996, **79**, 93–96.
19 M. Gaal, E. J. W. List and U. Scherf, *Macromolecules*, 2003, **36**, 4236–4237.
20 X. O. Gong, P. K. Iyer, D. Moses, G. C. Bazan, A. J. Heeger and S. S. Xiao, *Adv. Funct. Mater.*, 2003, **13**, 325–330.
21 Y. Shirota, *J. Mater. Chem.*, 2000, **10**, 1–25.
22 X.-H. Zhou, J.-C. Yan and J. Pei, *Org. Lett.*, 2003, **5**, 3543–3546.
23 A. L. Kanibolotsky, R. Berridge, P. J. Skabara, I. F. Perepichka, D. D. C. Bradley and M. Koeberg, *J. Am. Chem. Soc.*, 2004, **126**, 13695–13702.
24 B. Li, J. Li, Y. Fu and Z. Bo, *J. Am. Chem. Soc.*, 2004, **126**, 3430–3431.
25 W. Y. Lai, Q. Y. He, R. Zhu, Q. Q. Chen and W. Huang, *Adv. Funct. Mater.*, 2008, **18**, 265–276.
26 W.-Y. Lai, R. Zhu, Q.-L. Fan, L.-T. Hou, Y. Cao and W. Huang, *Macromolecules*, 2006, **39**, 3707–3709.
27 F. Liu, W.-Y. Lai, C. Tang, H.-B. Wu, Q.-Q. Chen, B. Peng, W. Wei, W. Huang and Y. Cao, *Macromol. Rapid Commun.*, 2008, **29**, 659–664.
28 D. Katsis, Y. H. Geng, J. J. Ou, S. W. Culligan, A. Trajkovska, S. H. Chen and L. J. Rothberg, *Chem. Mater.*, 2002, **14**, 1332–1339.
29 M. Sun, Y. Fu, J. Li and Z. Bo, *Macromol. Rapid Commun.*, 2005, **26**, 1064–1069.
30 Q. D. Liu, J. P. Lu, J. F. Ding, M. Day, Y. Tao, P. Barrios, J. Stupak, K. Chan, J. J. Li and Y. Chi, *Adv. Funct. Mater.*, 2007, **17**, 1028–1036.
31 C. Liu, Y. H. Li, Y. Y. Zhang, C. L. Yang, H. B. Wu, J. G. Qin and Y. Cao, *Chem.–Eur. J.*, 2012, **18**, 6928–6934.
32 C. F. Wang, W. Y. Hung, M. H. Cheng, J. S. Hwang, M. K. Leung and K. T. Wong, *Org. Electron.*, 2013, **14**, 1958–1965.
33 Y. Kuwabara, H. Ogawa, H. Inada, N. Noma and Y. Shirota, *Adv. Mater.*, 1994, **6**, 677–679.
34 R. Grisorio, G. Allegretta, P. Mastrorilli and G. P. Suranna, *Macromolecules*, 2011, **44**, 7977–7986.
35 E. J. W. List, R. Guentner, P. S. de Freitas and U. Scherf, *Adv. Mater.*, 2002, **14**, 374–378.
36 V. N. Bliznyuk, S. A. Carter, J. C. Scott, G. Klarner, R. D. Miller and D. C. Miller, *Macromolecules*, 1999, **32**, 361–369.
37 B. Chen, J. Ding, L. Wang, X. Jing and F. Wang, *Chem. Commun.*, 2012, **48**, 8970–8972.
38 Y. Tao, Q. Wang, Y. Shang, C. Yang, L. Ao, J. Qin, D. Ma and Z. Shuai, *Chem. Commun.*, 2009, 77–79.
39 T. Qin, W. Wiedemair, S. Nau, R. Trattnig, S. Sax, S. Winkler, A. Vollmer, N. Koch, M. Baumgarten, E. J. W. List and K. Müllen, *J. Am. Chem. Soc.*, 2011, **133**, 1301–1303.
40 E. Guillén, J. Hierrezuelo, R. Martinez-Mallorquin, J. M. Lopez-Romero and R. Rico, *Tetrahedron*, 2011, **67**, 2555–2561.
41 B. Chen, J. Q. Ding, L. X. Wang, X. B. Jing and F. S. Wang, *Chem. Commun.*, 2012, **48**, 8970–8972.
42 J. Ding, Q. Wang, L. Zhao, D. Ma, L. Wang, X. Jing and F. Wang, *J. Mater. Chem.*, 2010, **20**, 8126–8133.
43 H. Meier, U. Stalmach and H. Kolshorn, *Acta Polym.*, 1997, **48**, 379–384.
44 G. Schwartz, M. Pfeiffer, S. Reineke, K. Walzer and K. Leo, *Adv. Mater.*, 2007, **19**, 3672–3676.
45 X. Cao, Y. Wen, Y. Guo, G. Yu, Y. Liu and L.-M. Yang, *Dyes Pigm.*, 2010, **84**, 203–207.
46 Y. Liu, M. Nishiura, Y. Wang and Z. Hou, *J. Am. Chem. Soc.*, 2006, **128**, 5592–5593.